Journal of Alloys and Compounds 501 (2010) 77–84

Contents lists available at ScienceDirect

Journal of Alloys and Compounds

journal homepage: www.elsevier.com/locate/jallcom

Multiwall carbon nanotubes purification and oxidation by nitric acid studied by the FTIR and electron spectroscopy methods

L. Stobinski[a,b], B. Lesiak[a,*], L. Kövér[c], J. Tóth[c], S. Biniak[d], G. Trykowski[d], J. Judek[e]

[a] Institute of Physical Chemistry, Polish Academy of Sciences, Kasprzaka 44/52, 01-224 Warsaw, Poland
[b] Faculty of Materials Science and Engineering, Warsaw University of Technology, Wołoska 141, 02-507 Warsaw, Poland
[c] Institute of Nuclear Research, Hungarian Academy of Sciences (ATOMKI), H-4001 Debrecen, P.O. Box 51, Hungary
[d] Faculty of Chemistry, Nicolaus Copernicus University, Gagarina 7, 87-100 Toruń, Poland
[e] Faculty of Physics, Warsaw University of Technology, Koszykowa 75, 00-662 Warsaw, Poland

ARTICLE INFO

Article history:
Received 17 January 2010
Received in revised form 29 March 2010
Accepted 2 April 2010
Available online 13 April 2010

Keywords:
Multiwall carbon nanotubes
Purification
Functionalization
FTIR
Raman
Electron spectroscopy methods

ABSTRACT

A process of wet chemical purification, oxidation and functionalization of multiwall carbon nanotubes (MWCNTs) is investigated to determine the structural and chemical changes in atomic bonding caused by oxidation in an aqueous solution of concentrated (68%) HNO_3 at 120 °C. The original and oxidized multiwall carbon nanotubes (ox-MWCNTs) are studied using TEM, SEM, elemental analysis, mass spectrometry, EDX, FTIR, Raman and electron spectroscopy methods. The proposed wet chemical purification and modification of "as-prepared" MWCNTs, contaminated with amorphous carbon, catalyst supports and metallic catalysts removes effectively all impurities (traces of Al, Fe and amorphous carbon) resulting from the catalytic reaction applied for synthesizing the "as-prepared" MWCNTs. The proposed wet chemical purification of MWCNTs changes their hydrophobic nature to hydrophilic.

1. Introduction

The carbon nanotubes (CNTs) are carbon allotropes consisting of C sp^2 hybridizations, like graphene [1]. They exist in a wide variety of forms, *i.e.* single wall (SWCNTs), double wall (DWCNTs) and multi wall (MWCNTs) carbon nanotubes, where the cylindrical concentric planes interact with each other due to the van der Waals forces. MWCNTs are promising material for many technological applications considering their unique structure and possibility of modifications influencing their physical and chemical properties. Due to their large specific surface area and conductivity, MWCNTs can be successively applied as a support for metallic catalysts in electrooxidation reaction in fuel cells [2–4], other variety of reactions [5] and gas storage [6].

The modifications of MWCNTs material deal with several problems. First, the "as-prepared" synthesized material requires purification, *i.e.* removing amorphous carbon, traces of catalysts and catalysts supports. Such procedures, based on chemical and electrochemical reactions, result in obtaining a material containing C defects, *i.e.* sp^3-hybridized C atoms and other carbon, oxygen and hydrogen groups [7–12], and metallic nanoparticles [13]. Then, different chemical modification methods, depending on the required products, are carried out [7–13]. This aim may be achieved using wet chemical reactions, usually with aqueous solution of HNO_3, H_2SO_4, HCl or their mixtures, oxidation in ozone, oxygen, oxygen plasma and electrochemical reaction [7–11,13]. Functionalized MWCNTs, containing oxygen groups, were found to be more active than nonfunctionalized MWCNTs. Surface groups attached to MWCNTs and surface defects are the active sites for other functionalizations and catalytic reactions [5]. Obtaining the material with reduced number of defects proceeds usually under annealing [11,12].

The process of wet chemical purification, oxidation and functionalization of multiwall carbon nanotubes is investigated. The aim is to determine the chemical and structural changes between the original "as-prepared" carbon nanotubes and the MWCNTs chemically oxidized by the concentrated HNO_3 at 120 °C, denoted as ox-MWCNTs. The MWCNTs are studied by the transmission electron microscopy (TEM), elemental analysis, energy dispersive spectroscopy (EDX), Fourier transform infra-red spectroscopy (FTIR), Raman and electron spectroscopy methods, *i.e.* X-ray photoelectron spectroscopy (XPS), X-ray Auger electron spectroscopy (XAES), elastic peak electron spectroscopy (EPES) and reflection electron energy loss spectroscopy (REELS).

* Corresponding author. Tel.: +48 22 343 3432; fax: +48 22 632 52 76.
E-mail address: blo@ichf.edu.pl (B. Lesiak).

0925-8388/$ – see front matter © 2010 Elsevier B.V. All rights reserved.
doi:10.1016/j.jallcom.2010.04.032

2. Experimental

2.1. Samples

The "as-prepared" MWCNTs (CNT Co., LTD., Korea) were treated in boiling concentrated (68%) HNO_3 under a reflux condenser for about 50 h at 120 °C in order to remove amorphous carbon, traces of catalysts and their supports completely, and in addition to oxidize raw material. The oxidized MWCNTs (ox-MWCNTs) were successively eluted with deionised water, then by NH_4OH, water, HCl and again by deionised water until the pH of filtrate was stabilized.

2.2. Elemental analysis

The elemental analysis based on the complete and controlled combustion and the gas separation by means of the "purge and trap" method was performed using a Vario MACRO apparatus (Elementar Analysensysteme GmbH, Germany). The samples (20 mg) were heated for 12 h at 100 °C under atmospheric pressure, and then degassed at $p = 10^{-4}$ Pa for 12 h at RT. After catalytic combustion at 900 °C in oxygen atmosphere the content of carbon, nitrogen and hydrogen were determined from CO_2, NO_2 and H_2O. The oxygen content was determined from what was left after oxidation.

2.3. SEM/EDX

The scanning electron microscope (SEM), type 1430 VP (LEO Electron Microscopy Ltd., England), equipped with detectors of secondary electrons (SE), backscattered electrons (BSE) and an energy dispersive X-ray spectrometer (EDX) Quantax 200 with a detector XFlash 4010 (Bruker AXS Microanalysis GmbH, Germany), were applied to determine surface and subsurface (up to 5 μm depth) morphology and for quantitative measurements at RT.

2.4. Mass spectrometry (ICP-MS)

The content of metals (Fe and Al) in MWCNTs was measured by the mass spectrometry (ICP-MS), Agilent 7500. The following MWCNTs demineralization procedure was applied: 10 mg of MWCNTs was poured into 8 ml of concentrated, ultra-pure 65% HNO_3 and 2 ml of 30% hydrogen peroxide, and then placed in a microwave oven for 20 min at 200 °C.

2.5. FTIR

The transmission FTIR measurements were performed using a Fourier transform spectrometer (Spectrum 2000, Perkin Elmer, Germany) in the wavenumbers range of 700–4000 cm^{-1}. Before, the samples were heated at $p = 10^{-3}$ Pa and 150 °C, to remove water. The measurements of MWCNTs–KBr mixtures 1:300 proceeded at room temperature (RT).

2.6. Raman spectroscopy

Raman spectra were recorded using a Dilor spectrometer (XY 800) and the excitation wavelength was of λ = 514.5 nm. The typical resolution of peak position using micro-Raman system equipped with a 50× objective is about ±1 cm^{-1}. In order to exclude the temperature effects a very small laser power of about 0.1 mW was applied. The Raman spectra were base line corrected using a linear function and afterwards both the peak position and linewidth were determined by fitting to a Lorentzian function.

2.7. XPS/XAES, EPES and EELS, REELS

The electron spectra were measured in UHV using the ESA-31 spectrometer [14] equipped with a high resolution energy analyzer, an electron gun and X-ray excitation source. The XPS and XAES spectra were excited using AlK_α X-rays. The XPS, XAES and the respective REELS spectra were recorded using the fixed retardating ratio (FRR) working mode with retarding ratios 4, 8 and 16, at an X-ray beam incidence angle of 70° with respect to the surface normal and the emitted electrons were detected in the direction of the surface normal. The EPES and the respective REELS spectra were measured using FRR working mode equal to 32, the primary electrons kinetic energy *KE* of 2000 eV, a spot diameter of 1.5–2.0 mm, a current of 5.2–5.7 nA, at an incidence angle of 50° with respect to the surface normal and electrons emitted in the direction normal to the surface.

3. Results

3.1. SEM, TEM, elemental analysis, EDX, mass spectrometry (ICP-MS) and XPS

Comparison of morphology of "as-prepared" MWCNTs and ox-MWCNTs by SEM is given in Fig. 1. The exemplary TEM image of ox-MWCNTs is shown in Fig. 2. For the ox-MWCNTs the TEM and SEM images indicate the bundled structure of MWCNTs of diameters ranging from 10 to 40 nm. At the surface of "as-prepared" MWCNTs an amorphous carbon is observed by TEM (Fig. 2a). The oxidation treatment results in removing the amorphous carbon from nanotubes (Figs. 1b and 2).

The quantitative surface analysis by XPS was performed using the relative sensitivity factor method [15], whereas the EDX analysis by the semi-quantitative approach. The results of quantitative elemental analysis, EDX, mass spectrometry (ICP-MS) and XPS, indicating the presence of C, N, O, H, Al and Fe, with an increasing content of H and O after oxidation, are compared in Table 1. Within its surface sensitivity of about 5 μm the EDX of MWCNTs shows the presence of Al and Fe resulting from the MWCNTs synthesis. After purification and oxidation no traces of Al and Fe are observed by the EDX method. Since in the semi-quantitative EDX analysis the content of low atomic number elements is usually overestimated, the results on C, N and O are not included. The mass spectrometry confirms the presence of Fe and Al for "as-prepared" MWCNTs. The XPS spectroscopy, within its average surface sensitivity of about 5 nm, indicates at the surface of "as-prepared" sample only C, O and Al. No Fe is observed, due to the surface layer of amorphous carbon attenuating the signal of Fe 2p photoelectrons. After oxidation, Al and Fe are removed. Then, the traces of N and Cl are observed. The content of O in ox-MWCNTs increases significantly in comparison to the "as-prepared" nanotubes.

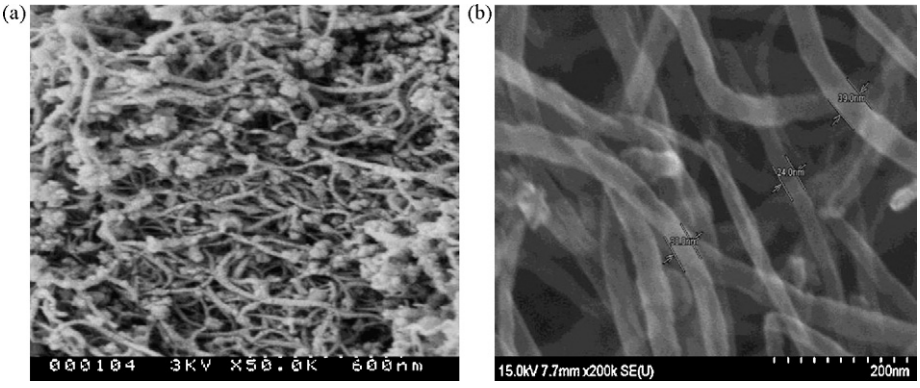

Fig. 1. Comparison of (as) "as-prepared" MWCNTs (600 nm) and (b) oxidized MWCNTs (200 nm) by SEM. The quantities given in brackets indicate the lateral resolution applied.

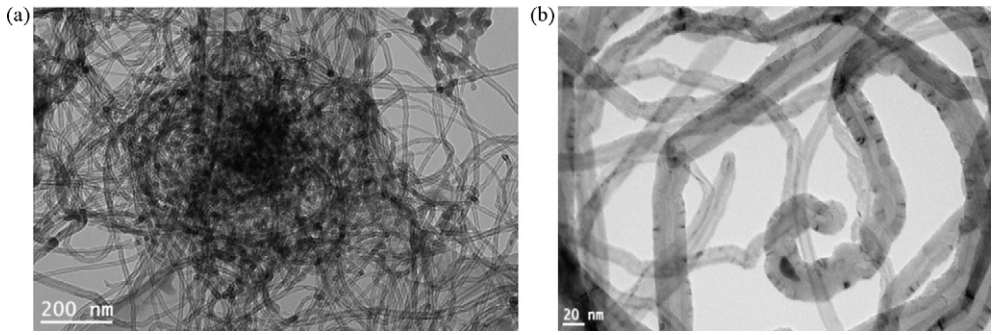

Fig. 2. TEM image of oxidized, bundled MWCNTs. Scale bars are for (a) 200 nm and (b) 20 nm.

Table 1
Comparison of weight percent values resulting from various analyses. Dash symbol indicates the elements which cannot be detected and are burdened by a large systematic error of a specific experimental method.

Elements	Analysis—content (wt%)							
	Elemental		EDX		ICP-MS		XPS	
	"As-prepared" MWCNTs	Ox-MWCNs	"As-prepared" MWCNTs	Ox-MWCNs	"As-prepared" MWCNTs	Ox-MWNCs	"As-prepared" MWCNTs	Ox-MWCNs
C	96.7	89.1	–	–	–	–	97.8	85.0
N	0.8	0.8	–	–	–	–	0	1.0
O	2.3	9.6	–	–	–	–	1.7	13.4
H	0.2	0.5	–	–	–	–	–	–
Cl	0	0	0	0	–	–	0	0.6
Al	0	0	0.6	0	0.2	0	0.5	0
Fe	0	0	1.9	0	0.6	0	0	0

3.2. FTIR

The FTIR spectra of "as-prepared" and oxidized MWCNTs are compared in Fig. 3. The spectra indicate intensive bands at wavenumbers 3444 cm^{-1} (stretching vibrations of isolated surface –OH moieties and/or –OH in carboxyl groups and in sorbed water). The shifts in characteristic wavenumbers in the direction of lower wavenumbers indicate the presence of strong hydrogen bonds between –OH groups. The bands in the 1750–1550 cm^{-1} range can be assigned to C=O groups in different environments (carboxylic acid, ketone/quinone) and to C=C in aromatic rings, whereas the bands in the range of 1300–950 cm^{-1} prove the presence of C–O bonds in various chemical surroundings. A band of wavenumbers at 1550 cm^{-1} most probably due to aromatic and unsaturated structural of ⟩C=C⟨ bonds, band near 1410 cm^{-1} due to sorbed water (OH in-plane deformation) and overlapping bands in region characteristic for C–O moiety (*e.g.* ⟩C–O–C⟨ groups—oxides of structural, oxygen bridges, etc.) are present in the FTIR transmission spectra of "as-prepared" multiwall carbon nanotubes.

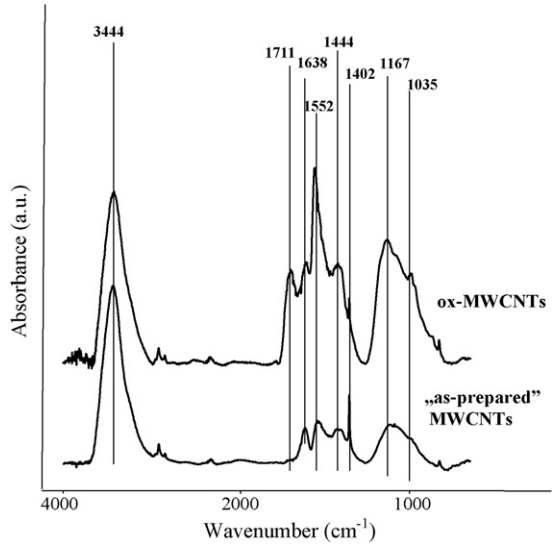

Fig. 3. The FTIR spectra of "as-prepared" and oxidized MWCNTs.

As a result of functionalization, the decreasing relative intensity of the –OH band assigned to the associated water (3444 cm^{-1}) and the appearance of an additional peak (near 3190 cm^{-1}) confirm the presence of various hydroxyl moieties at the carbon surface. The C=O bands characteristic of carboxyl functional groups (–COOH) and of ketone/quinone are observed at 1711 and 1638 cm^{-1}, respectively [16]. The relative increase and partial separation of bands in the 1250–950 cm^{-1} wave region points on increase in the amounts of hydrated surface oxides (O–H deformation and C–O stretching combination in surface phenols, hydroquinones and aromatic carboxylic acids).

3.3. Raman spectra

The Raman spectra, comparing "as-prepared" MWCNTs and oxidized MWCNTs, are shown in Fig. 4. They consist of the main G band at about 1580 cm^{-1} related to E_{2g} graphite mode and indicating C–C stretching vibrations, and two disorder-induced bands—D at about 1340 cm^{-1} and D′ at about 1620 cm^{-1} reflecting the high density of states for zone-edge and midzone phonons, respectively [17,18]. Moreover, second-order 2D feature at about 2700 cm^{-1} is observed for both samples and the C–H stretching vibration at 2920 cm^{-1} for oxidized samples only. The detailed structure of the D and G bands is presented in Fig. 4b, where peak positions as well as linewidth (in brackets) are shown. First, about double increase of intensity for disorder-induced bands is observed. The intensity ratios I_D/I_G or $I_{D'}/I_G$ equal to 0.75 and 0.09 for the "as-prepared" sample, and to 1.44 and 0.2 for the oxidized samples, respectively. The small values could be attributed to an increased number of sp^3-hybridized carbons in ox-MWCNTs. The linewidth

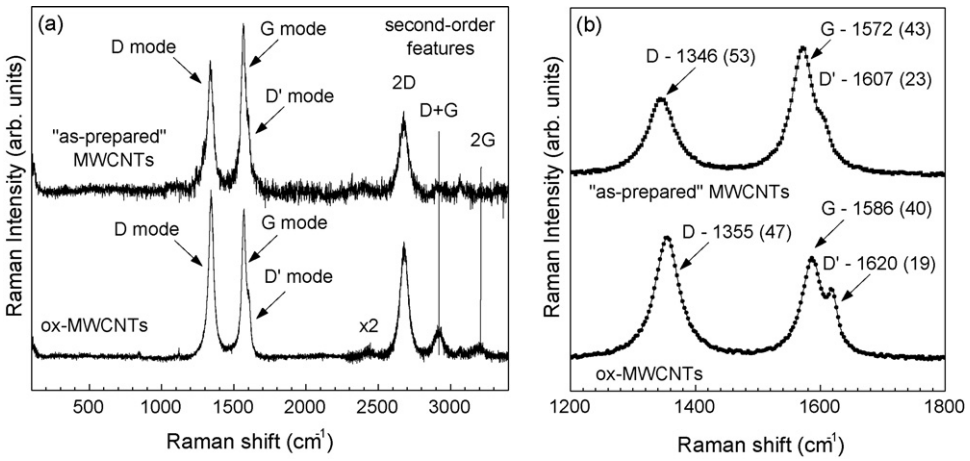

Fig. 4. The Raman spectra of "as-prepared" and oxidized MWCNTs.

of the studied modes slightly decreased following oxidation, which could be attributed to a smaller amount of amorphous carbon. A large shift of the G mode (+14 cm^{-1}) is observed suggesting changes in the MWCNTs electrochemical structure [19], *e.g.*, by the change of the amount and type of chemical groups attached to ox-MWCNTs walls/edges [20] or/and increased oxygen content in the nanotubes framework that acts as p-type dopant.

3.4. XPS and XAES chemical bond information

The energy positions for the C 1s, O 1s, N 1s, Cl 2p and Al 2p photoelectron lines on the binding energy (*BE*) scale measured in the case of "as-prepared" and oxidized MWCNTs, assigned to relevant chemical forms are indicated in Table 2. The assigned *BE* values from the literature [15,21,22] refer to the predominant atomic chemical form contributing to the maximum of XPS peak intensities (Table 2). The *BE* of C 1s electrons for "as-prepared" and oxidized samples at 284.4 eV indicates the predominance of C sp^2 bonds. The O 1s photoelectrons indicate a *BE* shift from 533 to 532 eV after oxidation. The *BE* at about 533 eV indicates O–C bonds in ethers and phenols, whereas the *BE* at about 532 eV the –O=C bonds in quinines, ketones and aldehydes. Since oxygen atoms in ester, carboxyl, anhydride and pyrone groups have both the single and double bonds with carbon, the oxygen atoms in these groups contribute to the above photoelectron lines. The larger contribution at about 533 eV, following oxidation, indicates the increasing content of carboxyl, acid anhydride and ester group defects in ox-MWCNTs. The *BE* of N 1s and Cl 2p electrons at 399.6 and 200.2 eV, respectively, cannot be attributed to nitrogen or chlorine bound to carbon [15,9,23], but rather to an organic matrix environment [15,21,22].

The content of carbon and oxygen groups at the surface of "as-prepared" and oxidized MWCNTs was evaluated from the C 1s and O 1s transitions using the software XPSPEAK41 [24]. After subtracting the Tougaard background, the measured C 1s and O 1s spectra were fitted to Gaussian–Lorentzian sum function with the parameters for the asymmetric tail, TS = 0.5 and TL = 10 [24]. The *BE* values for carbon and oxygen groups were taken from the literature [15,21–23,9,25,26]. For the C 1s sp^2 and C sp^3 hybridizations the experimental and theoretical value of *BE* difference equal to 0.9 eV remains consistent [25,26]. The *BE* values and the results of fitting into components for "as-prepared" and oxidized MWCNTs are indicated in Fig. 5a and b, respectively.

The results of the fitting procedure applied to the C 1s and O 1s spectra are given in Table 3. The atomic bond contributions are recalculated into the carbon and oxygen weight percents resulting from quantitative analysis by XPS applying the values from Table 1. For the C 1s line, under oxidation, the decrease of the C sp^2 hybridization contribution was observed, accompanied by the increase of the contribution from the carbon–oxygen groups, *i.e.* carbonyl, ester, carboxyl and acid anhydride. Similar increase of the contribution of the carbon–oxygen groups after oxidation was observed in the case of O 1s line (Table 3). In the Auger C KLL spectra the *BE* values for pπ and pσ electrons are separated by about 5 and 8 eV. The changes of carbon hybridization content in graphite (C sp^2), diamond (C sp^3) and amorphous carbon (C sp^2 and C sp^3 mixture) result in the modification of XAES spectra shape and the width of the first derivative spectra [25]. As reported in Ref. [25], the Auger C KLL first derivative spectrum line width can be described by a distance between the maximum and the minimum, called a parameter *D*, whereas the linear interpolation of parameter *D* for graphite and diamond allows for evaluating the C sp^2 percent. The respective C KLL spectra, values of parameter *D* and the C sp^2 content for "as-prepared" and oxidized MWCNTs are shown in Fig. 6. After oxidation the decrease of C sp^2 content from 86% to 80% can be observed.

3.5. XPS, EPES and EELS, REELS

The electron inelastic and elastic scattering processes reflected in the EELS and REELS spectra in the vicinity of the XPS lines and EPES spectra, respectively, can be applied for characterization of material surfaces. From the higher energy loss part of the spec-

Table 2
The experimental values of *BE* of XPS peaks assigned to atomic chemical forms.

XPS peaks	"As-prepared" MWCNTs		ox-MWCNTs	
	BE (eV)	Assignment	*BE* (eV)	Assignment
C 1s	284.4	Graphite	284.4	Graphite
O 1s	533.0	O–C in ethers, phenols	532.3	O=C in quinones, ketones, aldehydes
N 1s	–		399.6	N in organic matrix
Cl 2p	–		200.2	Cl in organic matrix
Al 2p	75.5	Al in organic matrix	–	

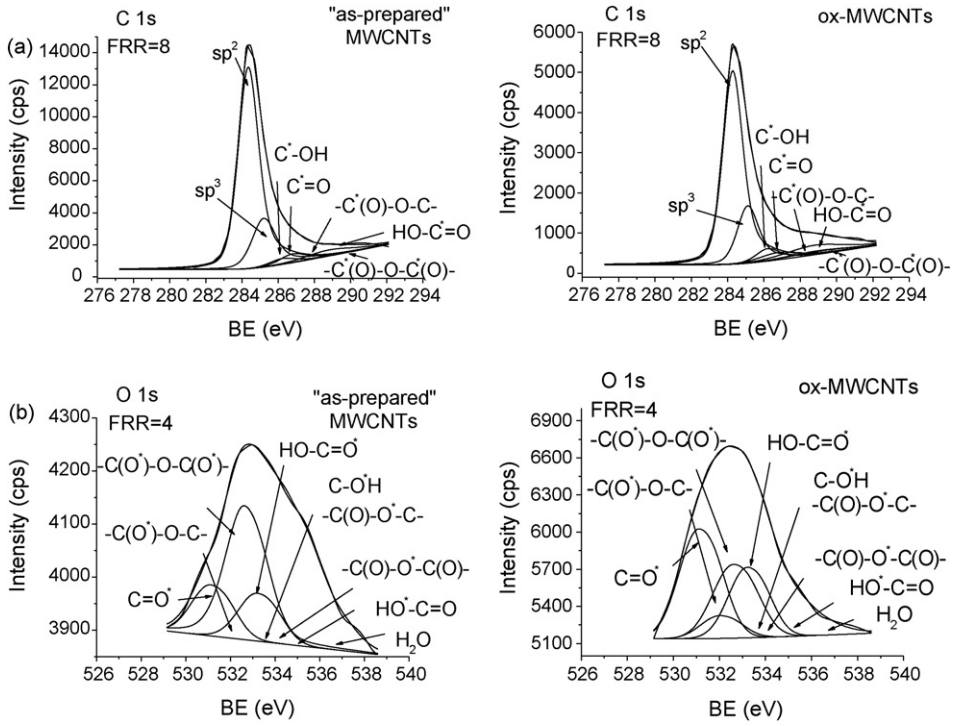

Fig. 5. Fitting of asymmetric Gaussian–Lorentzian functions to XPS spectra measured in the case of "as-prepared" and oxidized MWCNTs. (a) C 1s and (b) O 1s peaks.

tra usually the C sp^2 fraction of the material can be evaluated, whereas the low energy loss spectra allows for deriving the density of valence electrons and the material density [27,28]. Similarly to the case of the highly oriented pyrolitic graphite [29], the spectra full width at half maximum (FWHM) of the energy loss peak and its asymmetry may reflect the structural changes at the surface. As reported previously [27,28], REELS can be applied for characterization of surface properties from the energy and intensity associated with π and $\pi+\sigma$ loss peaks. Applying the dielectric model and a phenomenological approach within the free electron approximation, quantities like the density of valence electrons, n_{val}, density of material, ρ and the C sp^2 can be derived [27]. In the free electron approximation the value of n_{val} can be evaluated from the equation:

$$n_{val} = \frac{m}{4\pi e^2} E_p = 7.25 \times 10^{20} E_{\pi+\sigma}^2, \quad (1)$$

where m is an electron mass, e is an electron charge and $E_{\pi+\sigma}$ is the energy of $\pi+\sigma$ loss peak. Then, the value of ρ is:

$$\rho = \frac{n_{val} M_a}{N_A n_c}. \quad (2)$$

where M_a is the atomic weight, N_A the Avogadro number and n_c the number of valence electrons per carbon atom. Assuming only the C sp^2 and C sp^3 hybridizations, the fraction of the C sp^2 can be evaluated from [27]:

$$\frac{\text{C sp}^3}{\text{C sp}^2} = \frac{0.23 E_{\sigma+\pi}^2}{4E_\pi^2} - 1, \quad (3)$$

where E_π is the π plasmon energy and 0.23 is a screening factor taking into account the screening of π electrons. Also, the general expression for the relationship between the density and the C sp^3 fraction derived by Ferrari for a-C:H films [28] can be applied for

Table 3
Comparison of atomic bond contributions (weight percents) resulting from fitting of asymmetric Gaussian–Lorentzian functions to the measured C 1s and O 1s photoelectron peaks.

C 1s (FRR = 8)			O 1s (FRR = 4)		
Chemical bond	"As-prepared" MWCNTs (wt%)	Ox-MWCNTs (wt%)	Chemical bond	"As-prepared" MWCNTs (wt%)	Ox-MWCNTs (wt%)
sp^2 C–C	66.7	49.1			
sp^3 C–C	18.7	15.3			
C*–OH hydroxyl, phenol	2.3	3.7	C–O* H–C(O)–O*–C–	0	0
C*=O carbonyl	4.1	3.8	C=O*	0.2	4.1
–C*(O)–O–C– ester	5.0	7.6	–C(O*)–O–C–	0	0.8
HO–C*=O carboxyl	0	2.9	HO–C=O*	0.2	2.5
–C*(O)–O–C*(O)– acid anhydride	1.0	2.6	HO*–C=O	0.5	1.8
			–C(O*)–O–C(O*)–	0.6	2.9
			–C(O)–O*–C(O*)–	0	0.9
			H_2O	0.2	0.4

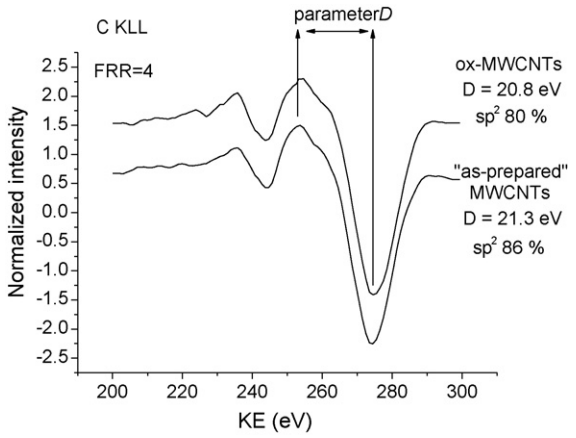

Fig. 6. The C KLL XAES first derivative spectra indicating in the width (parameter *D*) the percent of C sp^2 bonds for "as-prepared" and oxidized MWCNTs.

evaluating the surface material density:

$$\rho = 1.92 + 1.37C\ sp^3 \quad (4)$$

The XPS EELS and EPES REELS spectra recorded from "as-prepared" and oxidized MWCNTs are compared in Fig. 7a and b, respectively.

Comparison of selected parameters, like FWHM, π and $\pi+\sigma$ loss peak energies, the ratios of area under the π and $\pi+\sigma$ loss peaks, for the respective XPS EELS and EPES REELS spectra recorded from "as-prepared" MWCNTs and ox-MWCNTs, is listed in Table 4. These values were evaluated by fitting the spectra to Gaussian–Lorentzian sum function with the parameters for the asymmetric tail, following a Tougaard background subtraction [24]. The REELS spectra π plasmon energies from Table 4 were corrected for an electron recoil loss on C atom, which (for the applied primary electron energy of 2000 eV and measurement geometry) equals to 0.29 eV [30,31].

Comparison of MWCNTs surface parameters resulting from evaluating the XPS and EPES spectra experimental features (Table 4) is given in Table 5. The C sp^2 content values are estimated from the parameter *D* (Fig. 6) [25], the fitting of C 1s spectra (Table 3) and loss peaks energy in C 1s EELS spectra (Eq. (3)) [27]. The values of the density of valence electrons, n_{val}, for investigated MWCNTs surfaces are evaluated from loss peak energy (Eq. (1)) [27], and the surface density from the general relationship between mass density and C sp^3 content derived by Ferrari et al. for carbon films [28] (Eq. (4)). No significant changes are observed in values of FWHM in EPES and C 1s spectra after MWCNTs oxidation (Table 4), what suggests no pronounced structural changes of surface atoms [29]. The energy values for π loss peak resulting from C 1s EELS and REELS spectra indicate a decrease under oxidation, whereas the energy values of $\pi+\sigma$ excitation for C 1s EELS show an increase (Table 4). The intensity ratios of π peak to main peak indicate an increase under oxidation, whereas for $\pi+\sigma$ peak a decrease is observed (Table 4). Under oxidation, the MWCNTs surface parameters show a decrease of C sp^2 content accompanied by the increase of surface density (Table 5). The surface densities obtained from the C sp^2 content resulting from various approaches remain in agreement (Table 5). However, the respective surface densities are larger than the bulk densities resulting from the helium pycnometry measurement (Table 5).

4. Discussion and conclusions

The proposed method of a wet chemical purification and oxidation of "as-prepared" MWCNTs resulted in obtaining the high purity bulk, without traces of Fe and Al catalysts, modified ox-MWCNTs terminated by C attached to the oxygen groups, *i.e.* carboxyl, hydroxyl, carbonyl, ether, ester and acid anhydride, as confirmed by FTIR. The presence of these groups at the surface was also indicated by XPS.

The quantitative elemental analysis, EDX and XPS, indicated increasing content of O upon oxidation (Table 1). Wet chemical purification and oxidation resulted in the enhancement of sp^3-hybridized C atoms attached to the oxygen and/or hydrogen groups (Table 3, Figs. 4 and 6). An increase of oxygen groups (carbonyl, hydroxyl, carboxyl, ester, acid anhydride) attached to carbon was observed under oxidation (Table 3, Figs. 3 and 5). The chemical oxidation resulted also in structural changes visible in the electron inelastic loss region of EELS and REELS spectra, and increasing of the MWCNTs density (Tables 4 and 5, Fig. 7). All results were confirmed by the bulk FTIR, Raman, the surface XPS, XAES, EELS, REELS and helium pycnometry analyses. As shown elsewhere [12], the reduction of defects and the ox-MWCNTs reconstruction can be obtained by the modification changing the temperature.

The discrepancies between different approaches result from several sources, like the sensitivity and accuracy of the experimental methods applied and assumptions of models evaluating the chemical and physical quantities. The sensitivity and accuracy of the experimental methods applied is selective towards different components and restricted by the physical effect detected by the particular detector. The elemental analysis is possible for quantification of low atomic number elements, *i.e.* H, C, N, whereas for the elements like Al and Fe the ICP-MS, EDX and XPS are more convenient. The elemental content of Al and Fe by the EDX results from the semi-quantitative approach and is burdened by the error of several percent. The XPS method applying the sensitivity factors approach, assuming a homogeneous distribution of atoms in the solid and neglecting elastic electron scattering, results in an error of several percent [15]. However, among the quantitative methods applied, the evaluation of H content is possible using the elemental analysis. The quantification of H content with high accuracy is possible utilizing the effect of energy shift of the peak in the EPES spectra from electrons backscattered quasi-elastically on recoiled atoms of different atomic numbers [30]. Such effect was observed in polyethylene, consisting of C and H atoms, where the energy loss of electrons backscattered quasi-elastically (recoil shift) causes splitting of the elastic peak into two components enabling to estimate the surface concentration of H [31,32]. This energy splitting depends on the kinetic energy of electrons and the geometry of measurement [30]. For incident electrons kinetic energy of 2000 eV, the value of 3.6 eV was reported [31,32]. For the experimental conditions applied, in MWCNTs the electron quasi-elastic recoil shift for C, N, O and Cl atoms is smaller than the FWHM of the elastic peak at 2000 eV (Table 4, Fig. 7b), *i.e.* from 0.04 to 0.2 eV [30]. The H component of the elastic peak in the EPES spectra, shifted from the C component by 3.28 eV to the low energy side, is overlapped with the inelastic loss peak on π electrons (Table 4, Fig. 7b). The Raman spectroscopy and FTIR methods do not quantify the bulk content of C sp^2/sp^3 and other chemical carbon–oxygen–hydrogen groups, but indicate and compare qualitatively the existing groups after different sample treatment (Figs. 3 and 4). The quantification of chemical groups content is possible by XPS and XAES (Figs. 5a and b and Fig. 6, Tables 3 and 5). In the case of C 1s and O 1s spectra fitting (Fig. 5a and b), the accuracy of quantitative results depends on: (i) the background subtraction procedure influencing the measured area under the peak [24], (ii) the values of *BE* assumed for the spectra fitting [15,21,22] and (iii) the accuracy of the model (*e.g.* the sensitivity factor method) applied for quantitative analysis. Applying the Tougaard background subtraction [24], the same values of *BE* and FWHM and the sensitivity factor method [15], the error of evaluation does not exceed several percent. The accuracy of C sp^2/sp^3 content evaluated from C 1s and C KLL spectra is limited, respectively, by the assumed *BE* and the parameter *D* values,

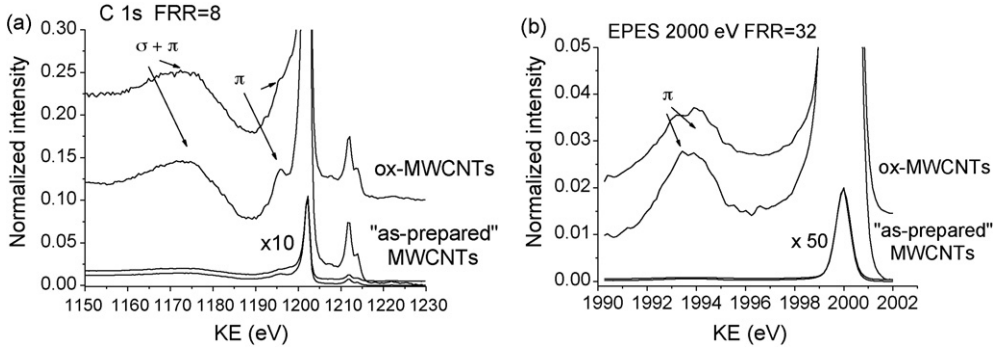

Fig. 7. Comparison of spectra from "as-prepared" and oxidized MWCNTs. (a) XPS EELS, (b) EPES REELS.

Table 4
Comparison of FWHM of EPES and XPS spectra, π and π + σ loss peak energy shifts, ratio of area under loss peak of REELS and XPS EELS spectra recorded from "as-prepared" MWCNTs and oxidized MWCNTs.

Sample	EPES REELS 2000 eV (FRR = 32)			XPS C 1s EELS (FRR = 8)				
	FWHM (eV)	π (eV)	A_π/A_{EPES} (%)	FWHM (eV)	π (eV)	π + σ (eV)	$A_\pi/A_{C\,1s}$ (%)	$A_{\pi+\sigma}/A_{C\,1s}$ (%)
"As-prepared" MWCNTs	0.69	6.86	5.07	1.53	6.68	28.96	23.69	43.98
Ox-MWCNTs	0.67	6.48	4.19	1.54	5.20	29.48	33.16	34.80

Table 5
Comparison of C sp^2 content, surface and bulk density resulting from different methods in "as-prepared" MWCNTs and oxidized MWCNTs.

Sample	C sp^2 (%)			$n_{val} \times 10^{17}$ (eV) (Eq (1))	ρ (g cm^{-3})			
	C KLL parameter D (FRR = 4)	C 1s fitting (FRR = 8)	Eq. (3) REELS (FRR = 8)		Surface (Eq. (4))			Bulk
					CKLL	C 1s	REELS	He pycnometry
"As-prepared" MWCNTs	86	78	93	6.08	2.11	2.22	2.02	1.950 ± 0.005
Ox-MWCNTs	80	76	54	6.30	2.19	2.25	2.55	2.100 ± 0.002

which usually result from experiments. These respective values were compiled elsewhere [33 and references within]. The experimental value of C 1s spectra *BE* difference for C sp^2 and C sp^3 bonds is 0.8–1.35 eV, however majority reports indicate the value of 0.9 eV [22]. The reported values of parameter *D* in C KLL spectra are for nanocrystalline diamond (NCD): 13–16.4 eV and for highly oriented pyrolitic graphite (HOPG): 21.1–22.8 eV [33]. These values depend significantly on the sample cleanness, *i.e.* oxygen contaminations and the proper content of the C sp^2 or sp^3 bonds in graphite and NCD, respectively. Also, the dependence of parameter *D* from clean graphite of different crystallinity and grain sizes was reported [33]. The worst accuracy for the C sp^2 content is evaluated from the REELS spectra, applying assumptions of only C sp^2 and C sp^3 bonds at the surface (Eq. (3)). Otherwise, the respective values resulting from C 1s spectra fitting and the parameter D remain within the accuracy of several percent (Table 5). However, the structural changes visible in the loss peak energies in EELS and REELS spectra recorded from MWCNTs, are qualitatively consistent with respective features observed for a set of a-C:H films of increasing C sp^2 hybridization [34], confirm the C hybridization changes under oxidation (Table 4, Fig. 7). The C sp^3 content obtained for "as-prepared" and ox-MWCNTs by electron spectroscopy methods indicates a large number of defects in the aromatic ring structure. However, the investigated material contains large number of multiwall nanotubes with shells separated from each other by 0.34 nm, and the electron spectroscopy methods sample an in-depth volume enclosing several nanotubes walls. Also, the agreement between density values resulting from the evaluated C sp^2 content by Eq. (4), and measured using the helium pycnometry is within several percent (Table 5). The oxidized MWCNTs exhibiting larger content of C sp^3 hybridizations and carbon–oxygen–hydrogen groups are characterized by a larger density value.

The most important factor which should be considered in comparison of results of elemental analysis, ICP-MS, FTIR, Raman investigating the sample bulk, and the EDX and electron spectroscopy methods quantifying the surface, is their in-depth sensitivity. The surface sensitivity of EDX is of order of about 5 μm, whereas the electron spectroscopy methods surface sensitivity is of order of about 5 nm. Otherwise, the quantitative results of elemental analysis, EDX, ICP-MS and XPS are consistent (Table 1). The "as-prepared" MWCNTs show lower O content than ox-MWCNTs. Besides, no traces of Al and Fe are observed in the oxidized MWCNTs. The N and Fe at the surface of "as-prepared" MWCNTs are not detected by the XPS due to the layer of amorphous carbon, causing an attenuation of photoelectron signal of lower kinetic energy. The amorphous carbon was confirmed by TEM (Fig. 2).

As shown in the present work, the proposed wet chemical purification and modification of "as-prepared" MWCNTs, contaminated with amorphous carbon, catalyst supports and metallic catalysts removes effectively all impurities (traces of Al, Fe and amorphous carbon) resulting from the catalytic reaction applied for synthesizing the "as-prepared" MWCNTs.

Acknowledgements

The authors would like to thank to Dr A. Presz for the helium pycnometry measurement of MWCNTs samples density. This work was supported by the exchange project between Polish Academy of Sciences and Hungarian Academy of Sciences, Projects of the Polish Council for Science: NN507378235, the Development Grants for the years 2008–2011 (NR. 15-0011-04/2008, KB/72/13447/IT1-B/U/08). The authors L. Kövér and J. Tóth thank for support by the project OTKA-K67873.

References

[1] S. Iijima, Nature 354 (1991) 56–58.
[2] L. Stobinski, J. Mazurkiewicz, H.-M. Lin, P. Tomasik, J. Nanosci. Nanotechnol. 5 (2005) 2121–2127.
[3] A. Borodziński, G.C. Bond, Catal. Rev. 48 (2006) 91–144.
[4] A. Borodziński, G.C. Bond, Catal. Rev. 50 (2008) 379–469.
[5] P.H. Matter, U.S. Ozakan, Catal. Lett. 109 (2006) 115–123.
[6] M. Kaempgen, M. Lebert, S. Roth, M. Soehn, N. Nicoloso, J. Power Sources 180 (2008) 755–759.
[7] F. Avilés, J.V. Cauich-Rodríguez, L. Moo-Tah, A. May-Pat, R. Vargas-Coronado, Carbon 47 (2009) 2970–2975.
[8] V. Datsyuk, M. Kalyva, K. Papagelis, J. Parthenios, D. Tasis, A. Siouku, I. Kallitsis, C. Galiotis, Carbon 46 (2008) 833–840.
[9] W. Xia, Y. Wang, S. Bergsträβer, S. Kundu, M. Muhler, Appl. Surf. Sci. 254 (2007) 247–250.
[10] H. Ago, T. Kugler, F. Cacialli, W.R. Salaneck, M.S.P. Shaffer, A.H. Windle, R.H. Friend, J. Phys. Chem. B 103 (1999) 8116–8121.
[11] K. Behler, S. Osswald, H. Ye, S. Dimovski, Y. Gogotsi, J. Nanoparticle Res. 8 (2006) 615–625.
[12] S. Kundu, Y. Wang, W. Xia, M. Muhler, J. Phys. Chem. C 112 (2008) 16869–16878.
[13] K. Saminathan, V. Kamavaram, V. Veedu, A.M. Kannan, Int. J. Hydrogen Energy 34 (2009) 3838–3844.
[14] L. Kövér, D. Varga, I. Cserny, J. Tóth, K. Tőkési, Surf. Interface Anal. 19 (1992) 9–15;
Z.-M. Zhang, Z.-J. Ding, H.-M. Li, K. Tőkési, D. Varga, J. Tóth, Surf. Interface Anal. 38 (2006) 632–635.
[15] J.F. Moulder, W.F. Sticle, P.E. Sobol, K.D. Bomben, Handbook of X-ray Photoelectron spectroscopy, Perkin-Elmer Co., Eden Prairie, MN, 1992.
[16] S. Biniak, M. Pakuła, A. Świątkowski, M. Walczyk, in: A.P. Terzyk, P.A. Gauden, P. Kowalczyk (Eds.), Carbon Materials: Theory and Practice, Research Signpost, Trivandrum, Kerala, India, 2008, p. 51, Ch. 5.
[17] R.J. Nemanich, S.A. Solin, Phys. Rev. B 20 (1979) 392–401.
[18] T.C. Chieu, M.S. Dresselhaus, M. Endo, Phys. Rev. B 26 (1982) 5867–5877.
[19] M. Rao, P.C. Eklund, S. Bandow, A. Thess, Nature 388 (1997) 257–259.
[20] P.W. Chiu, G.S. Duesberg, U. Dettlaff-Weglikowska, S. Roth, Appl. Phys. Lett. 80 (2002) 3811–3813.
[21] G. Beamson, D. Briggs, High Resolution XPS of Organic Polymers. The Scienta ESCA 300 Database, J. Wiley and Sons, Chichester, 1992.
[22] C.D. Wagner, A.V. Naumkin, A. Kraut-Vass, J.W. Allison, C.J. Powell, J.R. Rumble Jr, in: NIST X-ray Photoelectron Spectroscopy Database, NIST SRD 20, ver. 3.5, Gaithersburg, 2000. http://srdata.nist.gov/xps.
[23] E. Raymondo-Pinero, D. Cazorola-Amoros, A. Linares-Solano, J. Find, U. Wild, R. Schloegl, Carbon 40 (2002) 597–608.
[24] R.W.M. Kwok, XPS Peak Fitting Program for WIN95/98 XPSPEAK Version 4.1, Department of Chemistry, The Chinese University of Hong Kong, rmkwok@cuhk.edu.hk; http://www.phy.cuhk.edu.hk/~surface/XPSPEAK/index.html.
[25] J.C. Lascovich, S. Scaglione, Appl. Surf. Sci. 78 (1994) 17–23.
[26] R. Haerle, E. Riedo, A. Pasquarello, A. Balderschi, Phys. Rev. B 65 (2000) 045101–45111.
[27] J.C. Angus, F. Jansen, J. Vac. Sci. Technol. A 6 (1988) 1778–1782.
[28] A.C. Ferrari, A. Libassi, B.K. Tanner, V. Stolojan, J. Yuan, L.M. Brown, S.E. Rodil, B. Kleinsorge, J. Robertson, Phys. Rev. B 62 (2000) 11089–11092.
[29] S. Lizzit, L. Petaccia, A. Goldoni, R. Larciprete, Ph. Hofmann, G. Zampieri, Phys. Rev. B 76 (2007) 153408–153414.
[30] D. Laser, M.P. Seah, Phys. Rev. B 47 (1993) 9836–9839.
[31] G.T. Orosz, G. Gergely, M. Menyhard, J. Tóth, D. Varga, B. Lesiak, A. Jablonski, Surf. Sci. 566 (2004) 544–548.
[32] B. Lesiak, J. Zemek, J. Houdkova, Polymer 49 (2008) 4127–4132.
[33] B. Lesiak, J. Zemek, J. Houdkova, A. Kromka, A. Jóźwik, Anal. Sci. 26 (2) (2010) 217–222.
[34] F. Barreca, A.M. Mezzasalma, G. Mondio, F. Neri, S. Trusso, Thin Solid Films 398–399 (2001) 228–232.